Chemical Engineering Journal 96 (2003) 105–116

Chemical Engineering Journal

www.elsevier.com/locate/cej

Characterization of dynamic behaviour in gas–solid turbulent fluidized bed using chaos and wavelet analyses

N. Ellis [a,*], L.A. Briens [b], J.R. Grace [a], H.T. Bi [a], C.J. Lim [a]

[a] *Chemical and Biological Engineering, University of British Columbia, 2216 Main Mall, Vancouver, BC, Canada V6T 1Z4*
[b] *Chemical and Biochemical Engineering, University of Western Ontario, London, Ont., Canada N6A 5B9*

Abstract

The hydrodynamics of fluidized beds of FCC particles in a column of diameter 0.29 m were investigated based on gauge and differential pressure signals, as well as optical voidage probe data for conditions approaching and beyond the onset of the turbulent fluidization flow regime. It is shown that any treatment of the system as a dense phase/dilute phase binary is oversimplified given the broad spectrum of properties and the lack of clear delineation between two separate phases. On the other hand, chaos analysis indicates complex bifractal behaviour, with two separate values of the Hurst exponent corresponding to different scales of motion, while wavelet analysis is successful in again decomposing signals into scales of motion associated with voids and separate particles.

Keywords: Fluidization; Non-linear dynamics; Time-series analysis; Chaos; Wavelet transform; Turbulent flow regime

1. Introduction

In spite of the prodigious research effort devoted to its study for over half a century, some aspects of fluidized bed hydrodynamics remain elusive. The turbulent fluidization flow regime, in particular, is subject to continuing uncertainty and controversy. A comprehensive review covering what is known about the turbulent regime was published recently [1].

One of the factors underlying the uncertainty with respect to the turbulent fluidization flow regime relates to the conceptual basis for investigation employed by different research groups. Whereas the bubbling, slug flow and fast fluidization flow regimes can all be viewed and modelled as consisting of two distinct phases (bubbles and surrounding dense phase emulsion in the first case, gas slugs and surrounding dense phase in the second, and clusters and surrounding gas in the latter), the turbulent regime presents a more complex structure. Several different conceptual bases are possible:

(a) A number of studies, e.g. [2–5] have assumed that the basic structure of bubbling fluidized beds, i.e., gas bubbles immersed in a solids-in-gas emulsion, can be extended into the turbulent fluidization flow regime. Effective bubble properties (e.g. void diameter, velocity and frequency) are then ascribed to the system, and the bed is treated as if it were a bubbling bed, albeit one with smaller, faster-moving voids.
(b) It is possible [6,7] to view at least some turbulent fluidized beds as being subject to intermittency at each location, where periods of bubbling and fast fluidization alternate with each other, and the fraction of time corresponding to the latter increases as the superficial gas velocity is increased through the range beginning at the onset of turbulent fluidization, usually designated U_c, and terminating at the velocity corresponding to the transition from turbulent to fast fluidization. A variant of this approach [8,9] is to statistically hybridize the different fluidization flow regimes, i.e., to probabilistically average properties from three limiting regime-specific models, one each applying to bubbling, turbulent and fast fluidization.
(c) For cases where neither (a) nor (b) turns out to be appropriate, it is possible to utilize concepts and methodologies developed for other complex flows (e.g. single-phase turbulent flows, gas–liquid churn/turbulent flow regime) to characterize the hydrodynamic patterns observed in the turbulent fluidization flow regime. Deterministic chaos analysis and wavelet analysis provide methodologies that can be adapted to fluidized beds. The ultimate goal of such tools is to provide a fundamental framework for representing and predicting the behaviour of fluidized beds over the entire spectrum of flow regimes.

* Corresponding author. Tel.: +1-604-822-1243; fax: +1-604-822-6003.
E-mail address: nellis@chml.ubc.ca (N. Ellis).

1385-8947/$ – see front matter © 2003 Elsevier B.V. All rights reserved.
doi:10.1016/j.cej.2003.08.017

Nomenclature

a_j	approximation coefficient at scale j (–)
AP	single-point pressure (referred to as gauge pressure) (kPa)
d_j	detailed coefficient at scale j (–)
DP	differential pressure (kPa)
h	expanded bed height determined by axial pressure profile (m)
h_0	initial static bed height (m)
H	Hurst exponent (–)
i	time index (–)
j	wavelet dilation scale (–)
k	wavevector/translation parameter (–)
pdf	probability distribution function
r	radial coordinate (m)
R	column radius (m)
R/S	rescaled range analysis (–)
$s(i)$	voidage signal (–)
U	superficial gas velocity (m/s)
U_c	transition velocity at which standard deviation of pressure fluctuations attains a maximum (m/s)
$w_j(k)$	wavelet coefficient (–)
z	axial distance above distributor (m)

Greek letters

ε	voidage (–)
ε_{mf}	voidage at minimum fluidization (–)
ε_{peak}	peak voidage value (–)
τ_H	subperiods (s)
$\psi_j(k)$	wavelet function in time space (–)
ψ_0	wavelet basis function (–)

This paper addresses some of these issues, in particular with respect to approaches (a) and (c) above. Based on local voidage fluctuations and pressure fluctuations measured in a column of diameter 0.29 m, we first examine whether or not a two-phase representation (approach (a) above) is capable of capturing the essence of the hydrodynamic behaviour. It is shown that there is no unambiguous way of distinguishing two phases and that, in fact, there is a broad and continuous spectrum of local voidages and phenomena which render the two-phase representation inappropriate as a descriptor or basis for modelling the turbulent fluidization investigated experimentally for FCC particles.

In view of this finding, we then turn our attention to (c) above, in particular to two analysis methods that may be promising, i.e., chaos and wavelet analysis. A number of research groups, e.g. [10–15] have demonstrated that chaotic analysis methods can provide useful insights and can distinguish among flow regimes with respect to fluidized bed and other multiphase systems. Given the highly non-linear behaviour, chaos analysis should be especially applicable to the turbulent fluidization flow regime. Over at least some range of conditions, chaotic analysis has suggested multifractal behaviour of gas-fluidized beds [16], indicating that the complex flow patterns can be disaggregated and considered as being composed of different scales of motion. Wavelet analysis provides another method of analysing multiphase systems including fluidized beds, with due consideration of different scales contributing to the complex overall waveforms, e.g. [15,17,18]. Through wavelet analysis, a one-dimensional time series is transformed into a two-dimensional region displaying wavelet coefficient amplitudes as a function of both time and frequency. This enables time localization of spectral components to be interpreted [19]. According to Ren et al. [20], local voidage measurements from a fluidized bed can be decomposed into three scales: micro-scale (particle and fluid), meso-scale (voids, two-phase structure), and macro-scale (equipment, global). Information from wavelet analysis should complement that obtained from other techniques.

2. Analysis method

Hurst [21] initiated a new method of analysis for time series of natural phenomena. This analysis involves calculating the average rescaled range $(R/S)_{\tau_H}$ for various values of subperiod length τ_H. The analysis was conducted carefully using a procedure developed and extensively tested by Briens et al. [22]. The R/S analysis was only one of many methods used to examine the signals. The results of the various methods are provided in Ellis [23]. A Hurst exponent, H, is estimated [22] by:

$$H = \frac{\mathrm{d}[\ln(R/S)_{\tau_H}]}{\mathrm{d}[\ln(\tau_H)]} \quad (1)$$

A time series can be characterized by its Hurst exponent that is always between 0 and 1. For a random process, there is no correlation between past and future increments and the exponent is 0.5. Exponents greater than 0.5 indicate persistence in the data where the trend in the time series, whether increasing or decreasing, will likely continue. On the other hand, $H < 0.5$ indicates antipersistence in the data where the trend will likely reverse itself [24,25].

In many cases, the slope of the log–log plot of $(R/S)_{\tau_H}$ vs. τ_H is different at small subperiod lengths than at large subperiod lengths, with a smooth transition between these two regions. Since the regions of interest are those where the slope H is constant, two Hurst exponents can be obtained. In addition, the dominant cycle of a signal can be estimated from the intercept of the two regions.

Many systems are chaotic and these can be plotted in phase space with the long-term evolution of the system forming a topological structure called an attractor. The most commonly utilized characteristic of an attractor is its correlation dimension. The correlation dimension indicates the complexity of the structure of the attractor in phase space [26–29]. A high correlation dimension corresponds to a

highly complex attractor with many degrees of freedom. The correlation dimension can be calculated by the Grassberger and Procaccia [30] algorithm using an embedding window length equal to the dominant cycle time [31].

In wavelet analysis, dilating or contracting the chosen analysing wavelet before convolving it with the signal accomplishes scale decomposition. The Daubechies wavelet [32] is utilized in this work for it has the highest number of vanishing moments for a given support width [33], ensuring that the signal analysis becomes more precise with the higher order of polynomials used for approximation. In the case of discrete wavelet transform, the dilation scale, j, and translation coefficient, k, take only discrete values. Filters of different cut-off frequencies are used to analyse the signal at different scales. The wavelet function can be expressed as:

$$\psi_j(k) = 2^{-j/2}\psi_0\left(\frac{k}{2^j}\right) \quad (2)$$

The discrete wavelet coefficients for the wavelet transform are

$$w_j(k) = \sum_{i=1}^{N}\psi_j(k - 2^j i)s(i) \quad (3)$$

where $s(i)$ is a time-series signal. An algorithm written in MATLAB© was used in this project to decompose the voidage signal using Daubechies 5th order wavelet, and to reconstruct signals at each scale from the wavelet coefficients [23].

3. Experimental technique

The 0.29 m diameter, 4.5 m tall Plexiglas vessel is equipped with 58 sampling ports. The distributor is an aluminium perforated plate containing 98 holes of 5.6 mm diameter arranged in an equilateral triangular configuration with a 32 mm pitch, resulting in an open area ratio of 3.7%. Solids circulation is not controlled, but rather determined through a pressure balance between the return leg and the column. There are two flapper valves installed in the return leg to prevent gas from escaping up the standpipe. Fluidizing air is supplied by a Roots blower with a maximum capacity of 425 N m^3/h at 69 kPa. Both steady-state and dynamic pressure measurements were obtained by 20 gauge and differential pressure transducers located at regular intervals along the column. Spent FCC particles of 78 μm mean diameter and density 1560 kg/m^3 constituted the fluidizing material. In order to alleviate electrostatic effects, the catalysts particles were mixed with approximately 0.5 wt.% of Larostat 519 particles, in addition to grounding the column at multiple points.

The two identical reflection type optical fibre probes, PC-4 Powder Voidmeter, used for voidage measurements in this work, were supplied by the Institute of Chemical Metallurgy of the Chinese Academy of Science in Beijing, China. The probe contains a bundle of fibres projecting light onto a swarm of particles interspersed with light-receiving fibres which measure the intensity of the light reflected from the particles. The bundle diameter is 4 mm, length is 600 mm, and individual fibre diameter is 15 μm. After placing a quartz glass window of 0.5 mm thickness on the probe tip, the optical fibre signal exhibited a very nearly linear response against the local voidage [23,34]. Both pressure and voidage data were logged using LABTECH© data acquisition software sampling at 100 Hz for periods of 100 s.

4. Results and discussion

4.1. Binary analysis

As previously reported [35], frequency analysis of pressure signals recorded in fluidized beds reveals dominant frequencies which characterize the flow regime. Analysis of the dominant peaks can be related to the physical behaviour, particularly in the bubbling and slugging flow regimes where the pressure fluctuations are a strong function of the movement of bubbles and slugs and when there is a clear bimodal distribution of voidage between bubbles and the surrounding emulsion phase. In analysing signals from turbulent fluidized beds, some reports have extended the analysis method of a bimodal distribution [36,37]. This approach is linked to case (a) discussed in Section 1, where the turbulent flow regime is simply treated as an extended bubbling regime. However, based on our extensive study on the hydrodynamics of turbulent fluidized beds, the treatment of the voidage distribution in this flow regime as 'bimodal' is questionable, given the breakdown of large bubbles into smaller transient voids, the expansion of the dense phase and the broad distribution of local instantaneous voidage.

Fig. 1 shows that the voidage distribution measured by an optical probe indicates both unimodal and bimodal

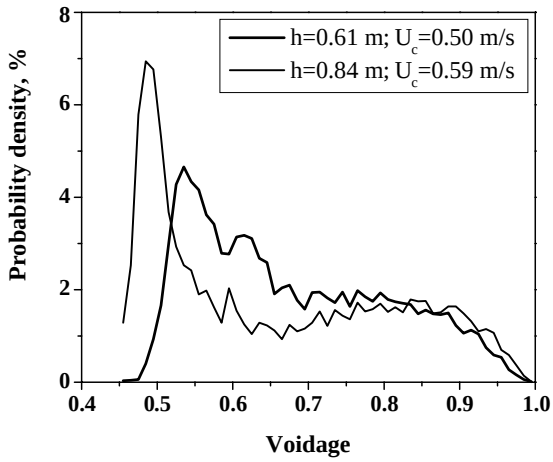

Fig. 1. Probability distribution of voidage measured by optical voidage probe. $U = 0.6$ m/s, $z = 0.27$ m, $r/R = 0.0$.

distributions, depending on the operating conditions and the location of the measuring probe. In all cases, the distributions are relatively flat, indicating continuous variation of voidage, rather than discrete values corresponding to two phases. In order to determine a crossing frequency from the local voidage fluctuation data or to extend the two-phase theory to a turbulent fluidized bed, it is required to choose a threshold voidage to delineate the boundary between the two phases. Given the continuous variation, the threshold voidage value in deducing the crossing frequency from the local voidage measurement becomes arbitrary and ambiguous.

The effect of the threshold value distinguishing two phases, determined through six different methods, on the resulting void velocity, calculated via binary coding, is explored in detail in Fig. 2. Examined previously by Bi and Su [38], Method (a) simply distinguishes the two phases according to whether the local voidage exceeds the mid-value between the maximum and minimum voidage signal values. The outliers, i.e., data which fall below $\varepsilon_{mf} = 0.45$ (for FCC) or above $\varepsilon = 1.0$ after conversion according to the calibration values, are removed before setting the maximum and minimum voidage values. Since, as discussed above, the signal has a linear relationship with voidage measured by our optical probe with a cover, the volume fraction of each phase corresponds to the area underneath the probability distribution function (pdf) curve on either side of the dividing line. Method (b), employed by Bayle et al. [39], sets the threshold value at the line indicated by the arrow shown in Fig. 2(b), i.e., at a voidage of $2\varepsilon_{peak} - \varepsilon_{mf}$. This method ensures that the threshold value lies above the maximum peak of a pdf. For Method (c), the threshold value is set at a point corresponding to 0.95 times the difference between the maximum and the minimum voidage signal, as proposed by Mainland and Welty [40] for a light-penetration type optical fibre probe. This method is clearly unsuitable for a reflective type optical fibre probe in a turbulent fluidized bed, as the dense phase voidage corresponding to the maximum peak of a pdf plot shifts toward a higher

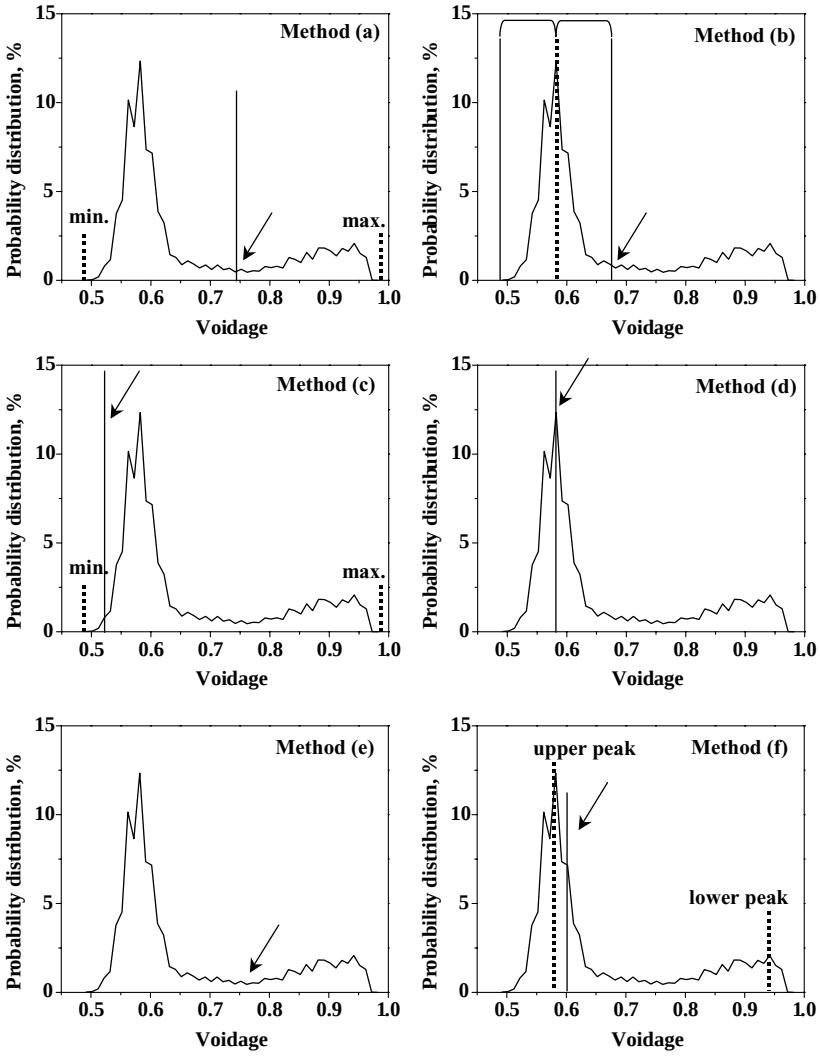

Fig. 2. pdf of local voidage measured by optical probe showing various threshold values corresponding to an imposed boundary between dilute and dense phases. $U = 0.69$ m/s, $z = 0.78$ m, $h_0 = 1.0$ m, $r/R = 0.55$.

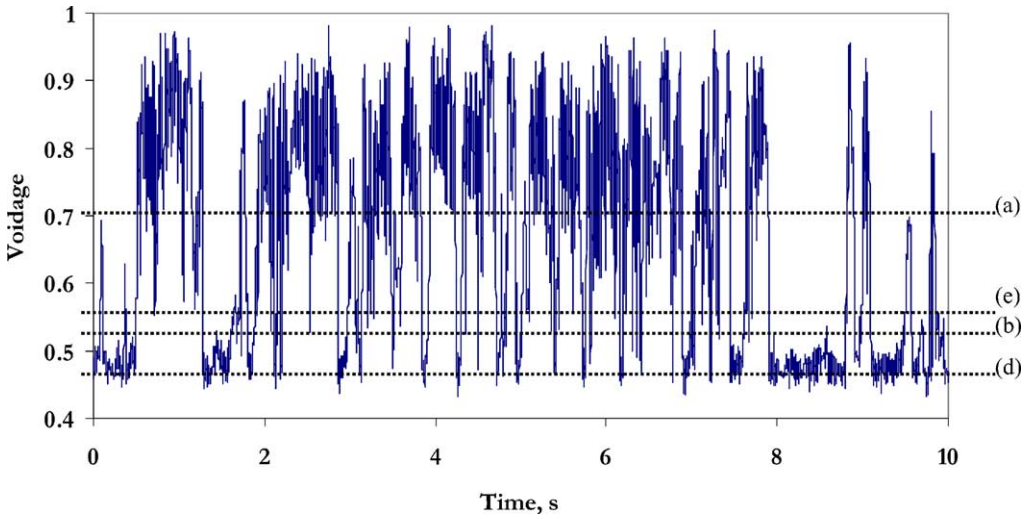

Fig. 3. Voidage fluctuations measured by optical voidage probe. $U = 0.69$ m/s, $z = 0.78$ m, $r/R = 0.70$.

voidage, and thus corresponds to no physically meaningful value.

The fourth method, illustrated in Fig. 2(d), uses the maximum peak of the pdf plot to demarcate the transition between the two phases. Method (e) is the minimum point cut method, proposed by Bi [41], which employs the minimum of the smoothed pdf plot as the dividing value. The determination of the threshold value then becomes ambiguous when the pdf curve becomes flat, especially for measurements near the wall. Moreover, it was difficult to mathematically express the minimum point when a smooth probability distribution was not obtained. The last method, shown schematically in Fig. 2(f), utilizes the value which corresponds to 0.95 times the difference between the two peaks to represent the value distinguishing a dense and dilute phase in a pdf plot. Once again, this method can involve large error when either peak is indistinct.

Local voidage data obtained from the optical voidage probe are plotted vs. time in Fig. 3, with four of the threshold values calculated from the above definitions (a, b, d and e) indicated by horizontal dotted lines. Method (c) has been excluded as being clearly inappropriate, while (f) is close to (d). Method (d) appears to use a threshold voidage which is unreasonably low, but there is no clear advantage or disadvantage of any of the other values. The effect of the threshold value on the crossing frequency is tabulated in Table 1. The results indicate that the crossing frequency from voidage fluctuations is very sensitive to the threshold determination method. This is a valuable insight, which suggests that the division of fluidized beds into discrete dense and dilute phases, while helpful for bubbling and slugging fluidized beds, may not be appropriate for turbulent beds. Any attempt to impose a threshold value between binary phases is arbitrary and affects the subsequent data analysis.

Table 1
Effect of threshold determination methods on voidage value and crossing frequency[a]

Threshold determination method	Threshold voidage	Crossing frequency (s^{-1})
Method (a)	0.704	22.0
Method (b)	0.527	5.86
Method (d)	0.475	23.7
Method (e)	0.565	6.31

[a] $U = 0.69$ m/s, $r/R = 0.70$, $z = 0.78$ m, $h_0 = 1.5$ m.

4.2. Chaos analysis

Given the failure of Method (a) in Section 1, we turn to alternative methods of analysis. While use of a discrete voidage corresponding to distinct dilute and dense phases is problematic, our data shown in Fig. 4, like those of several previous groups, do indicate bifractal behaviour when chaotic analysis methods are applied. The Hurst exponent at higher frequency, H_1, representing the slope at lower τ_H, is

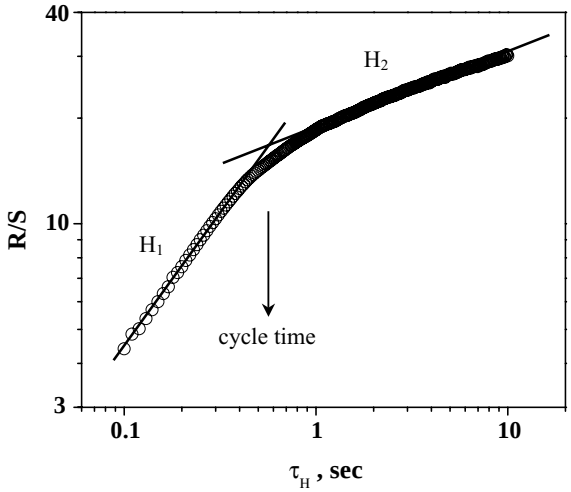

Fig. 4. Variation of rescaled range with subperiod length for pressure fluctuation. $U = 0.86$ m/s, $z = 0.59$ m, $h_0 = 1.5$ m.

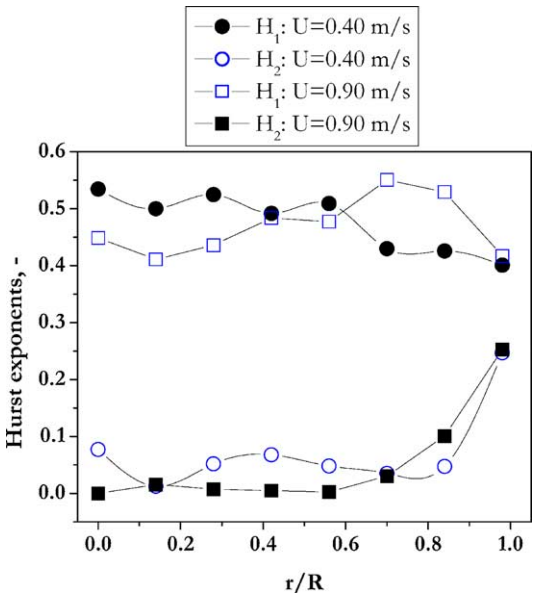

Fig. 5. Radial profile of Hurst exponents from optical probe signals at $U = 0.40$ and 0.90 m/s. $z = 0.78$ m, $h_0 = 1.1$ m, $U_c = 0.73$ m/s.

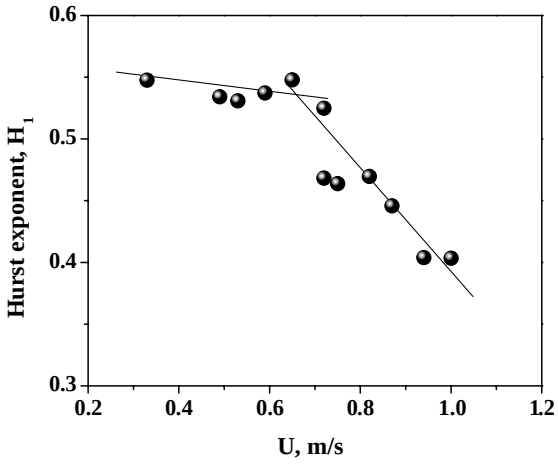

Fig. 6. Variation of the greater of the two Hurst exponents from optical probe signals with superficial gas velocity. $z = 0.40$ m, $U_c = 0.75$ m/s, $h_0 = 1.5$ m, $r/R = 0.0$.

found to be close to 0.5 for measurements in the bubbling flow regime, i.e., $U = 0.86$ m/s, indicating a pure Brownian motion. On the other hand, the Hurst exponent at lower frequency, H_2, representing the slope at larger τ_H, suggests that H_2 is much smaller than 0.5, portraying antipersistent behaviour.

Based on the rescaled range analysis method, Fig. 5 illustrates radial profiles of the Hurst exponents for $U = 0.40$ and 0.9 m/s calculated from Eq. (1). The Hurst exponent H_1, from the slope of $\log(R/S)_{\tau_H}$ vs. $\log(\tau_H)$ at lower τ_H (higher frequency) remains close to 0.5 for $U = 0.40$ m/s near the column axis, indicating random motion. Though their Hurst exponents were much higher, Bai et al. [13] reported a similar radial profile for the bubbling flow regime. However, their study indicated that in the turbulent fluidization flow regime, both Hurst exponents, H_1 and H_2 exceeded 0.5, increasing towards the wall. Fig. 5 indicates smaller differences between the two Hurst exponents near the wall, implying less phase separation than in the core of the column.

As shown in Fig. 6, H_1 from local voidage measurements indicates a sudden drop with increasing superficial gas velocity, suggesting a change in the high frequency fluctuations. The velocity at which this abrupt drop occurs may correspond to the transition into the turbulent fluidization flow regime. The sensitivity of H_1 from voidage signals to the change in local fluctuations may suggest a viable means of deducing the transition velocity, U_c. However, this would suggest $U_c \approx 0.65$ m/s, while the usual method relating to the maximum of the standard deviation of gauge pressure fluctuations gives $U_c = 0.75$ m/s.

The cycle time calculated from the intercept of the two slopes of Hurst exponents, as illustrated in Fig. 4, represents a lag time caused by a dominant cyclic component of a signal [42]. The variation of the cycle time with the axial position of the pressure taps for differential and gauge pressure signals, DP and AP, appear in Fig. 7(a) and (b), respectively. Three superficial gas velocities are chosen as representative U values, corresponding to $U < U_c$, $U \approx U_c$, and $U > U_c$, where $U_c = 0.75$ m/s. For DP signals, Fig. 7(a), increasing U increases the cycle time for all superficial gas velocities close to the distributor, indicating gradual growth in voids due to coalescence with height. The range of cycle times of 0.3–0.55 s corresponds well to the dominant frequency detected from spectral analysis of DP signals of 1.5–3 Hz, as reported in [35]. At $z = 1.1$ m for $U = 1.0$ m/s, the trend in cycle time reverses, suggesting dominance of void splitting over coalescence. Above this point the bed becomes dominated by smaller voids, contributing to increased homogeneity of the turbulent fluidized bed.

The trend shown from gauge pressure signals, Fig. 7(b), indicates two distinct regions: one nearer the distributor corresponding closely to the natural frequency of the bed, and the other indicating much lower cycle times. As signals from gauge pressure reflect global phenomena in a fluidized bed, they may reflect the origin, propagation, and attenuation of pressure waves. Following the analysis of [41], the higher cycle time near the bottom of the fluidized bed may indicate pressure waves of much lower frequency than the natural frequency of the bed, implying that the bed is acting "as a wave propagation medium". On the other hand, at $z = 0.46$ m and beyond, the imposed pressure waves have frequencies higher than the natural frequency of the bed, resulting from oscillatory motion. Oscillations are dampened by energy loss from interparticle collisions, gas-particle drag and friction between the suspension and the wall, but sustained by the continuous supply of pressure waves. In a turbulent fluidized bed, it is extremely difficult, if not impossible, to pin-point all factors contributing to pressure fluctuations owing to the complex dynamics.

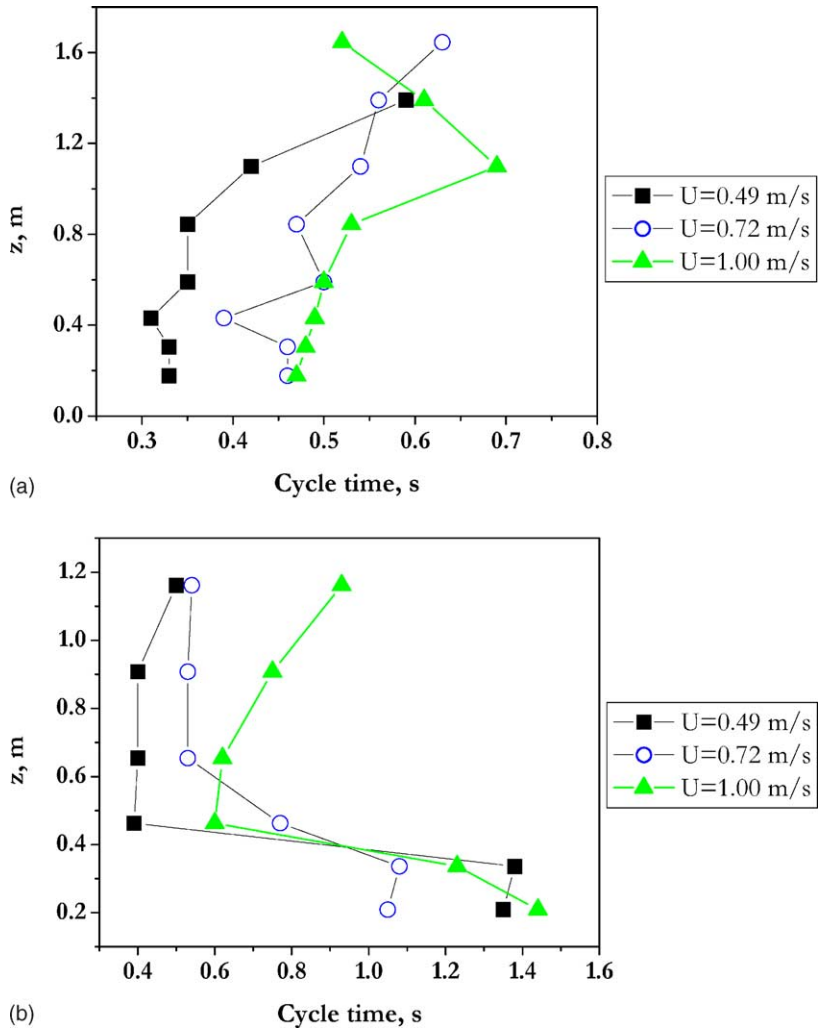

Fig. 7. Axial profiles of cycle time from (a) DP and (b) AP signals for $h_0 = 1.5$ m, $U_c = 0.75$ m/s, $r/R = 1.0$.

The cycle time deduced from rescaled range analysis for voidage signals is shown in Fig. 8. Considerable scatter of cycle time is observed, with no definite trend indicated, nor any obvious transition to match that shown in Fig. 6. The general trend of decreasing cycle time with increasing U indicates increasing cycle frequency of voidage fluctuations. The range of cycle frequency, i.e., reciprocal of cycle time, corresponds closely to the range of frequencies observed from FFT of DP signals, as previously reported [35].

Further chaotic analysis is applied to the DP measurements in Fig. 9 through the correlation dimension. Different trends in correlation dimension appear for the bubbling and turbulent fluidization flow regimes for pressure measurements closer to the distributor. Higher correlation dimensions near the distributor plate for $U > U_c$ can be attributed to the complexity of the structure of the attractor due to the vigorous motions of solids due to jetting. For $U = 0.33$ and 0.49 m/s, the variation of correlation dimension with height is similar. However, for $U > U_c$ at higher axial positions, sensitivity of correlation dimension to U is observed,

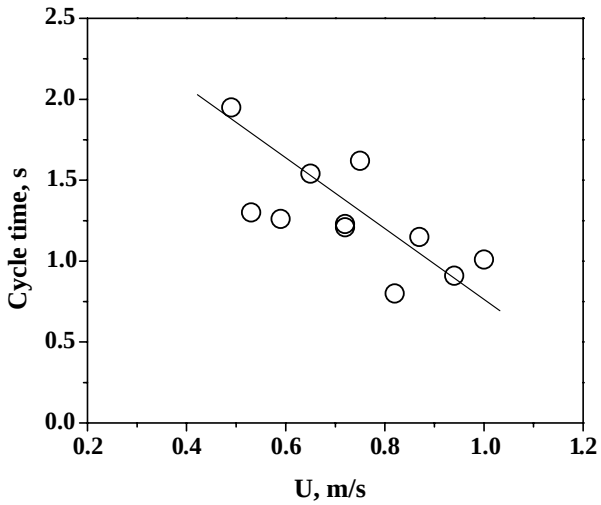

Fig. 8. Variation of cycle time with superficial gas velocity for optical voidage probe signals. $z = 0.40$ m, $r/R = 0.0$, $h_0 = 1.5$ m, $U_c = 0.75$ m/s.

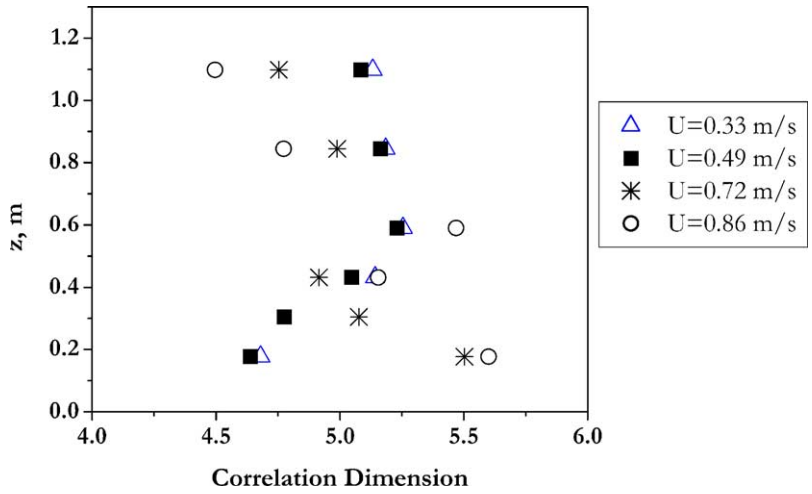

Fig. 9. Axial profiles of correlation dimension from DP signals. $h_0 = 1.5$ m, $U_c = 0.75$ m/s, $r/R = 0.0$.

possibly reflecting the transient flow structure in the turbulent fluidized beds. For example at $z = 0.85$ m, where the flow is well developed and the effect of the fluctuating bed surface is minimal, the correlation dimension decreases with increasing U, indicating a more coherent flow structure and increased homogeneity.

The radial distributions of the correlation dimension based on local voidage measurements at $U = 0.4$ and 0.9 m/s are shown in Fig. 10. There is considerable scatter, with the profiles appearing to rise towards the wall and generally lower correlation dimensions for $U > U_c$, suggesting less complex structure resulting from local voidage fluctuations in turbulent fluidized beds, in agreement with the findings of Bai et al. [13].

Although there is some scatter, Fig. 11 suggests that there is a correlation between the correlation dimension and the cycle time deduced from the rescaled range analysis of local voidage fluctuations. If we consider an attractor such as the Lorenz attractor in 3D space, the shape and the complexity of the attractor will affect the 'cycle' through which the system passes. Thus, if an attractor is quite large and complicated, i.e., it has a larger correlation dimension, this is likely to result in a larger cycle time, as a long time will be required for the trajectory to travel once around the general shape of the attractor. Similarly, a lower correlation dimension from the local voidage fluctuations of the turbulent fluidized beds implies less complexity of the structure of the attractor in the phase space and a shorter cycle time.

The error associated with the chaos analysis in deriving the parameters is considered to be minimal. Each point in the $\log(R/S)_{\tau_H}$ vs. $\log(\tau_H)$ graph is the average of many calculated points, e.g., 1000 points average at $\tau_H = 0.1$ s. Once stability is attained on a specific operating condition, the 95% confidence interval of the average pressure

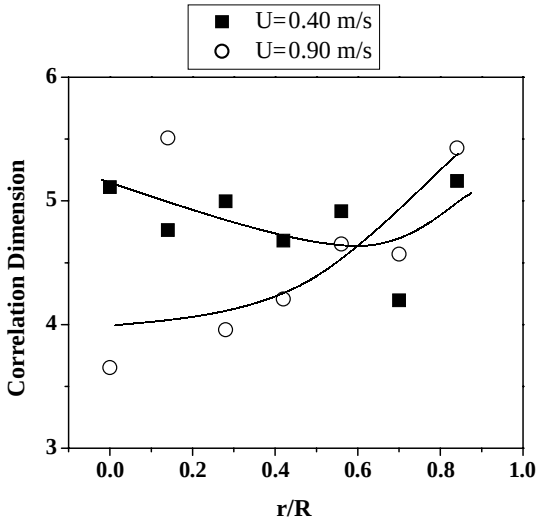

Fig. 10. Radial profile of correlation dimension from optical probe signals. $z = 0.78$ m, $h_0 = 1.1$ m, $U_c = 0.73$ m/s.

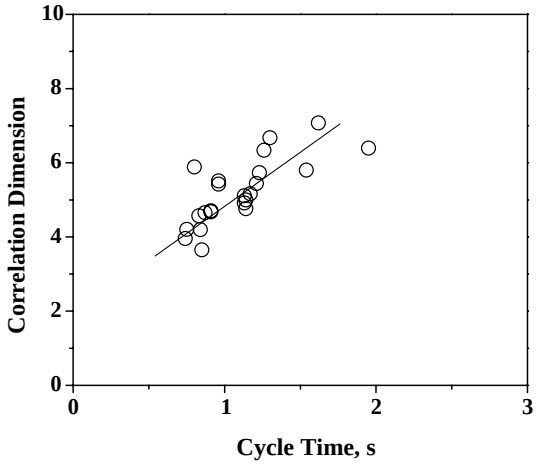

Fig. 11. Correlation between cycle time and correlation dimension from optical probe signals.

measurements ranges between ±0.22 and ±4.6% for AP and DP signals respectively. A typical set of DP signals indicate higher H_2 error % than H_1, i.e., ±17.6 vs. ±2.7%. This is due to the fewer points to fit the curve at low subperiod lengths. The resulting cycle time exhibited 95% confidence interval of ±5.1%. On the other hand, reproducibility of voidage signals from optical probes is lower than the pressure signals. This is due to the inherent fluctuations of the local voidage, especially in the turbulent fluidization flow regime. While H_1 exhibited a 95% confidence interval of ±3.7%, H_2 and the resulting cycle time had shown ±18.7 and ±75.4%, respectively. This supports the reproducibility of H_1, and the sensitivity towards the change in local voidage fluctuations, as shown in Fig. 6. On the other hand, cycle time based on voidage signals, in Fig. 8, should be presented as a general trend.

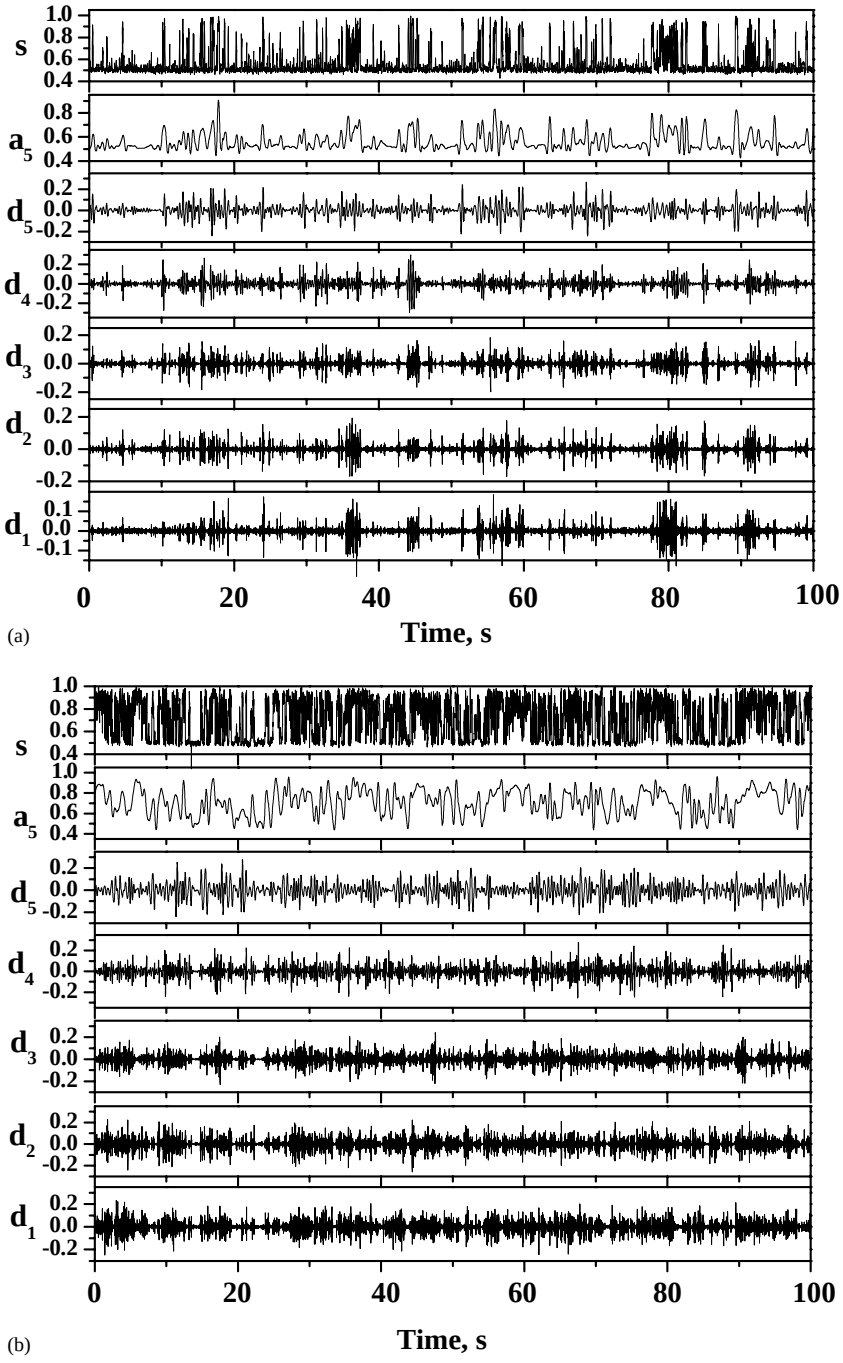

Fig. 12. Discrete wavelet decomposition of voidage fluctuation from optical probe using Daubechies 5 wavelet for (a) $U = 0.49$ m/s and (b) $U = 1.0$ m/s. $z = 0.4$ m, $h_0 = 1.5$ m, $U_c = 0.75$ m/s, $r/R = 0.0$.

4.3. Wavelet analysis

To gain better understanding of the dynamics of the local voidage fluctuations, data from the optical fibre probe sampled at 100 Hz have been analysed using the Daubechies 5 wavelet [32]. Through the wavelet transform, a signal is linearly decomposed into different scales related to frequency. Fig. 12 depicts the decomposed signal at five levels of detail and one approximation through discrete wavelet transformation. It was ensured that the reconstructed voidage signals displayed excellent agreement with the original signals. The intensities of the details d_1, d_2 and d_3 representing fine-scale components for $U = 1.0$ m/s are shown to be much higher than at $U = 0.49$ m/s, indicating intensified energy of the high frequency fluctuations, which are likely to originate from particle movement. Comparison of the approximations, a_5, between $U = 0.49$ and 1.0 m/s indicates increasing smoothness of the decomposition for the lower superficial gas velocity, possibly due to lower signal moments, i.e., lower order of the polynomial approximation. This results in smoothing out some of the singularities, such as isolated peaks, resulting from void movements in the signal. Taking the third and fourth statistical moments, Figs. 13 and 14, respectively, illustrate the dominance of the a_5 approximations for $U = 0.49$ m/s. In Fig. 13, the near-zero skewness of the decomposed signals for both superficial gas velocities display near-normal distributions. The higher skewness for the signal and approximation, a_5, at $U = 0.49$ m/s represent distributions that are heavily distributed toward the lower voidage compared to the higher voidage. The flatness of the distribution indicated by the kurtosis number in Fig. 14 represents constantly lower kurtosis value for $U = 1.0$ m/s. High kurtosis numbers (=3 for Gaussian distribution) may suggest intermittency for d_1 and d_2 at $U = 0.49$ m/s. From Fig. 12a, this is explained by high frequency energy, mostly associated with passing voids.

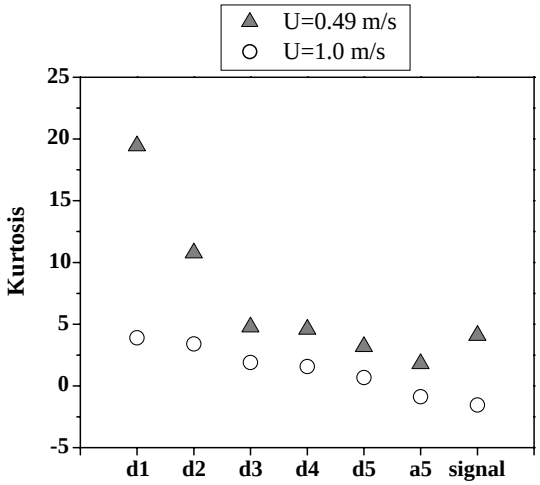

Fig. 14. Kurtosis distribution of decomposed voidage data presented in Fig. 11 using Daubechies 5 wavelet. $z = 0.4$ m, $h_0 = 1.5$ m, $U_c = 0.75$ m/s, $r/R = 0.0$.

Fig. 15 plots the larger Hurst exponent, H_1, for each of the details and approximations shown in Fig. 12. For the coarser-scale details, such as d_4 and d_5, and approximations, a_5, similar values of H_1 are observed for $U = 0.49$ and 1.0 m/s. Moreover, the difference remains at the fine-scale, high frequency fluctuations of d_1 and d_2, i.e., values of H_1 in the turbulent flow regime are less than in the bubbling regime. With H_1 values for d_1 and d_2 less than 0.5 for both superficial gas velocities, the fine-scale components indicate a convergent system which is likely to reverse itself. Further investigation is required to fully understand the implications of the results; however, this preliminary investigation using wavelet analysis indicates promising ways to decompose signals on the basis of different scales.

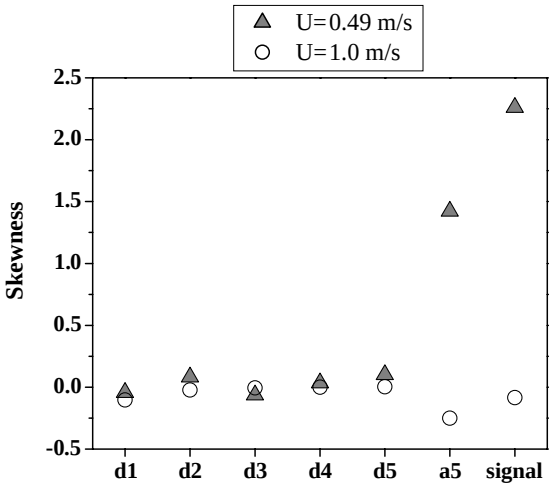

Fig. 13. Skewness distribution of decomposed voidage data presented in Fig. 11 using Daubechies 5 wavelet. $z = 0.4$ m, $h_0 = 1.5$ m, $U_c = 0.75$ m/s, $r/R = 0.0$.

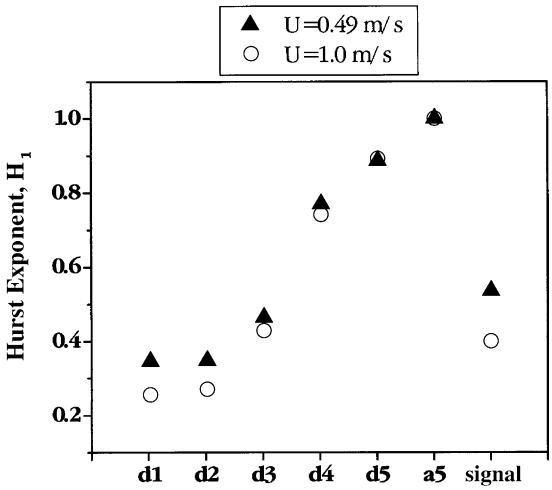

Fig. 15. Hurst exponent of decomposed voidage data presented in Fig. 11 using Daubechies 5 wavelet. $z = 0.4$ m, $h_0 = 1.5$ m, $U_c = 0.75$ m/s, $r/R = 0.0$.

5. Conclusion

From the experimental work involving measurements of gauge and differential pressure and local voidage in fluidized beds operated at conditions approaching and beyond the onset of turbulent fluidization flow regime, several approaches to the underlying idea understanding the complex flow have been explored. Treating data from a turbulent fluidized bed as a combination of co-existing discrete bubbles and dense phase was found to be inappropriate because the bed operating in this flow regime shows a broad spectrum of voidages and behaviour, with no clear delineation criteria between the two phases. On the other hand, both chaos analysis and wavelet analysis lead to the conclusion that there are differences between large- and small-scale motions in turbulent fluidized beds, opening the way for further investigation utilizing these tools to characterize this complex flow regime.

Acknowledgements

The authors are grateful for financial support from the Natural Sciences and Engineering Research Council of Canada (NSERC). We are also grateful to Cor van den Bleek who helped to interest us in chaos analysis as a tool for investigating fluidized beds.

References

[1] H.T. Bi, N. Ellis, I.A. Abba, J.R. Grace, A state-of-the-art review of gas–solid turbulent fluidization, Chem. Eng. Sci. 55 (2000) 4789–4825.
[2] R. Yamazaki, M. Asai, M. Nakajima, G. Jimbo, Characteristics of transition region in a turbulent fluidized bed, in: Proceeding of the Fourth China–Japan Fluidization Conference, Science Press, Beijing, 1991, pp. 720–725.
[3] H.I. Farag, P.E. Ege, A. Grislingas, H.T. de Lasa, Flow patterns in a pilot-scale fluidized bed reactor, Can. J. Chem. Eng. 75 (1997) 851–860.
[4] C. Lu, Y. Xu, M. Shi, F. Shen, Two-area model for bubble distribution in a turbulent fluidized bed of fine particles, Chin. J. Chem. Eng. 5 (1997) 287–295.
[5] J. Chaouki, A. Gonzalez, C. Guy, D. Klvana, Two-phase model for a catalytic turbulent fluidized-bed reactor: application to ethylene synthesis, Chem. Eng. Sci. 54 (1999) 2039–2045.
[6] H.T. Bi, J.R. Grace, K.S. Lim, Transition from bubbling to turbulent fluidization, Ind. Eng. Chem. Res. 34 (1995) 4003–4008.
[7] J.R. Grace, Reflections on turbulent fluidization and dense suspension upflow, Powder Technol. 113 (2000) 242–248.
[8] M.L. Thompson, H.T. Bi, J.R. Grace, A generalized bubbling/turbulent fluidized bed reactor model, Chem. Eng. Sci. 54 (1999) 2175–2185.
[9] I.A. Abba, J.R. Grace, H.T. Bi, M.L. Thompson, Spanning the flow regimes: a generic fluidized bed reactor model, AIChE J. 49 (2003) 1838–1848.
[10] C.S. Daw, J.S. Halow, Characterization of voidage and pressure signals from fluidized beds using deterministic chaos theory, in: E.J. Anthony (Ed.), Proceedings of the 11th Fluidized Bed Combustion Conference, ASME, New York, 1991, pp. 777–786.
[11] C.M. Van den Bleek, J.C. Shouten, Deterministic chaos: a new tool in fluidized bed design and operation, Chem. Eng. J. 53 (1993) 75–87.
[12] J.C. Schouten, M.L.M. van der Stappen, C.M. van den Bleek, Scale-up of chaotic fluidized bed hydrodynamics, Chem. Eng. Sci. 51 (1996) 1991–2000.
[13] D. Bai, A.S. Issangya, J.R. Grace, Characteristics of gas-fluidized beds in different flow regimes, Ind. Eng. Chem. Res. 38 (1999) 803–811.
[14] L.A. Briens, C.L. Briens, Cycle detection and characterization in chemical engineering, AIChE J. 48 (2002) 970–980.
[15] Q. Guo, G. Yue, J. Werther, Dynamics of pressure fluctuation in a bubbling fluidized bed at high temperature, Ind. Eng. Chem. Res. 41 (2002) 3482–3488.
[16] D. Bai, H.T. Bi, J.R. Grace, Chaotic behavior of fluidized beds based on pressure and voidage fluctuations, AIChE J. 43 (1997) 1357–1361.
[17] B.R. Bakshi, H. Zhong, P. Jiang, L.S. Fan, Analysis of flow in gas–liquid bubble columns using multi-resolution methods, Trans. I. Chem. E. 73 (1995) 608–614.
[18] X. Lu, H. Li, Wavelet analysis of pressure fluctuation signals in a bubbling fluidized bed, Chem. Eng. J. 75 (1999) 113–119.
[19] F. Hlawatsch, G.F. Boudeaux-Bartels, Linear and quadratic time-frequency signal representations, IEEE Signal Process. Mag. 9 (1992) 21–67.
[20] J. Ren, Q. Mao, J. Li, W. Lin, Wavelet analysis of dynamic behavior in fluidized beds, Chem. Eng. Sci. 56 (2001) 981–988.
[21] H.E. Hurst, Methods of using long-term storage in reservoirs, Trans. Am. Soc. Civil Engrs. 116 (1951) 770–808.
[22] C.L. Briens, L.A. Briens, J. Hay, C. Hudson, A. Margaritis, Hurst's analysis to detect minimum fluidization and gas maldistribution in fluidized beds, AIChE J. 43 (1997) 1904–1908.
[23] N. Ellis, Hydrodynamics of gas–solid turbulent fluidized beds, Ph.D. Thesis, University of British Columbia, Canada, 2003.
[24] J. Feder, Fractals, Plenum Press, New York, 1988.
[25] E.E. Peters, Applying Chaos Analysis for Investment and Economics, Wiley, New York, 1994.
[26] P.S. Addison, Fractals and Chaos: An Illustrated Course, IOP Publishing Ltd., London, UK, 1997.
[27] J. Thieler, Estimating fractal dimension, J. Opt. Soc. Am. 7 (1990) 1055–1072.
[28] M.L.M. van der Stappen, Chaotic hydrodynamics of fluidized beds, Ph.D. Thesis, Delft University, The Netherlands, 1996.
[29] R.C. Zijerveld, Chaotic hydrodynamics of large and small circulating fluidized beds, Ph.D. Thesis, Delft University, The Netherlands, 1998.
[30] P. Grassberger, L. Procaccia, Characterization of strange attractors, Phys. Rev. Lett. 50 (1983) 346.
[31] L. Briens, Identification of flow regimes in multiphase reactors by time series analysis, Ph.D. Thesis, University of Western Ontario, Canada, 2000.
[32] I. Daubechies, Ten lectures on wavelets, Soc. for Ind. and Applied Mathematics, Philadelphia, PA, 1992.
[33] MATLAB Documentation, Version 6.1, 2001.
[34] J. Liu, Particle and gas dynamics of high density circulating fluidized beds, Ph.D. Thesis, University of British Columbia, Canada, 2001.
[35] N. Ellis, J.R. Grace, C.J. Lim, H.T. Bi, K.S. Lim, Frequency analysis of pressure fluctuations in turbulent fluidized beds, in: J.R. Grace, J.-X. Zhu, H. de Lasa (Eds.), Proceedings of the Seventh International Conference on Circulating Fluidized Beds, Can. Soc. Chem. Eng., Ottawa, 2002, pp. 287–294.
[36] Q. Lin, F. Wei, Y. Jin, Transient density signal analysis and two-phase microstructure flow in gas–solid fluidization, Chem. Eng. Sci. 56 (2001) 2179–2189.
[37] I. Taxil, P. Guigon, F. Archimbault, T.A. Gauthier, Gas flow characterization in turbulent fluidization for FCC catalyst, in: L.-S. Fan, T.M. Knowlton (Eds.), Fluidization IX, Engineering Foundation, NY, 1998, pp. 69–76.
[38] H.T. Bi, P.C. Su, Local phase holdups in gas–solid fluidization and transport, AIChE J. 47 (2001) 2025–2031.

[39] J. Bayle, P. Mege, T. Gauthier, Dispersion of bubble flow properties in a turbulent FCC fluidized bed, in: M. Kwauk, J. Li, W.C. Yang (Eds.), Fluidization X, United Engineering Foundation, NY, 2001, pp. 125–132.
[40] M.E. Mainland, J.R. Welty, Use of optical probes to characterize bubble behavior in gas–solid fluidized beds, AIChE J. 41 (1995) 223–228.
[41] X.T. Bi, Flow regime transitions in gas–solid fluidization and transport, Ph.D. Thesis, University of British Columbia, Canada, 1994.
[42] L.T. Fan, Y. Kang, D. Neogi, M. Yashima, Fractal analysis of fluidized particle behavior in liquid–solid fluidized beds, AIChE J. 39 (1993) 513–517.